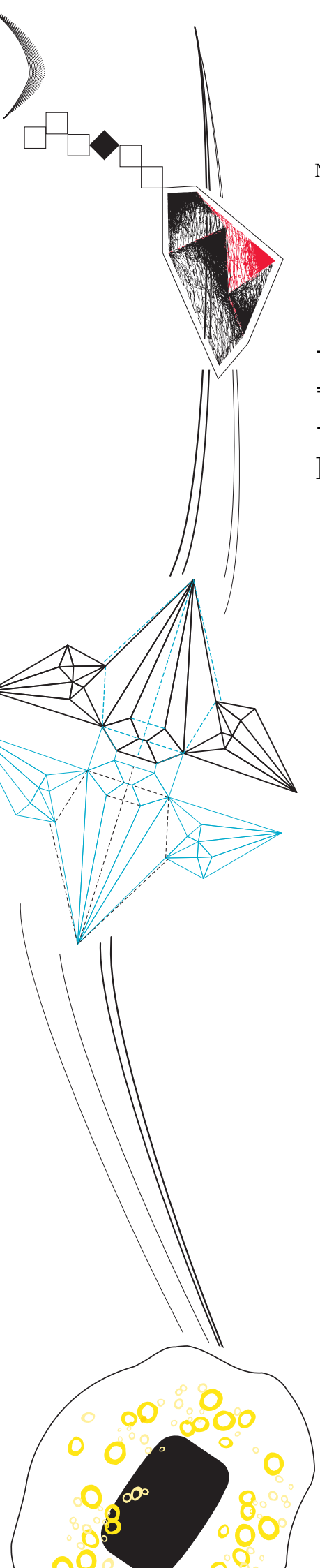

November 5, 2020

Design of a Mirror Manipulator

Free Space Optical Communication

Module 8 **Group 17**

Kevin Cacarin Cumbal	s2074311
David Carrera Robles	s2074222
Prudhvi Gali	s2061198
Kelvin Jaramillo Cordova	s2074206
Sameer Nizamudeen	s2065479
Pin Ni Yoong	s2161974

Tutor: Hakan Koroglu

UNIVERSITY OF TWENTE.

Version	1.0
Number of pages	13

Contents

Contents **i**

1 Concept **1**
1.1 Schematic Overview . . . 1
1.2 Requirements and Main Specifications . . . 1
1.3 Kinematic Structure . . . 2
1.4 Dynamic Parameters . . . 2
1.5 Control Parameters . . . 3

2 Design **4**
2.1 Mechanical Design . . . 4
2.2 CAD Model . . . 5
2.3 Frequency Response, Eigenfrequencies and Mode Shapes . . . 5
2.4 Controller Discretization . . . 6
2.5 Effects of Parasitic Dynamics, Controller Discretization, Sampling and Delay . . . 7
2.6 Design Limitations . . . 8

3 Implementation **8**
3.1 Controller (Simulink) . . . 8
3.2 Simulation Model of the Closed-Loop System . . . 8

4 Design Verification **9**
4.1 Static Gain and linearity . . . 9
4.2 Frequency response . . . 9
4.3 Discrete Controller . . . 10

5 Performance Verification **11**
5.1 Simulation results . . . 11
5.2 Comparison of simulation results and design analyses . . . 11
5.3 Verification of system performance . . . 11
5.4 Evaluation & Recommendations . . . 12

References **13**

Introduction

The goal of this project is to design a manipulator which steers a mirror that makes a communication laser track a satellite during a Free Space Optical (FSO) communication operation from ground to space. FSO communication is a technology that uses light to wirelessly transmit data for networking and telecommunications[1]. The report consists of five sections - *Concept*, *Design*, *Implementation*, *Design Verification*, and *Performance Verification*.

1 Concept

1.1 Schematic Overview

The concept depicted in Figure 1 is based on the structure with two steel plates which bend and introduce a rotation about the pivot point. The mirror is placed at this pivot point such that, no additional translational movement needs to be considered for kinematic calculations. Another advantage of the concept is that the position of the sensor and the voice coil motor (VCM) are aligned with the pivot point, thus, allowing to obtain the position of the encoder in a simplified way.

Description of symbols:

- L1: distance from the pivot to the sensor
- L2: distance from the pivot to the VCM
- L3 and L4: distances from pivot to action points of leaf springs 1 and 2
- k1 and k2: stiffness at the acting points of leaf springs 1 and 2
- L5 and L6: lengths of the leaf springs
- x: vertical displacement

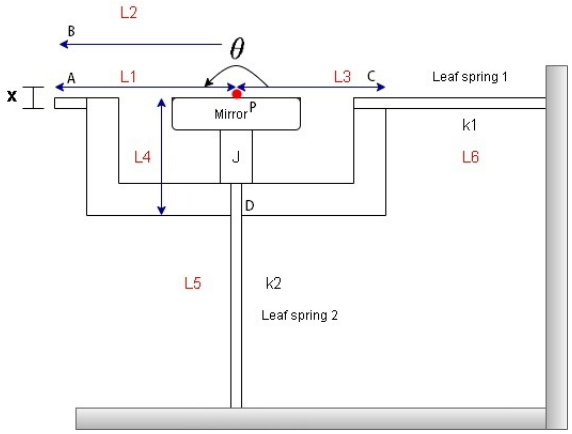

Figure 1: Schematic Overview of the mechanism (Side view)

Working principle

The VCM applies vertical force at point B, which causes a moment about the pivot point, P which has a moment of inertia J. At points C and D, the leaf springs apply reaction forces and moments. The encoder located at point A reads and displacement x, which can be used to calculate the angle of rotation ($\theta = \frac{x}{L1}$). (Note: Refer to Figure 1 for the labels).

1.2 Requirements and Main Specifications

Functional Requirements

- 1 DOF mechanical system
- Tracking accuracy of 25 μrad
- The satellite has to be tracked for around 2 seconds
- The system has to have robust stability (Nyquist plot is within the unit circle)

Hardware Specifications

- The VCM actuator AVM 30-15 (323772) provides a continuous force of 4.63 N with amplifier limited to 24 V.
- The collimated (parallel) laser beam is manipulated by a common mirror of 25.4 mm diameter

Additional Requirements

- The direction of the force has to be perpendicular to the line between the pivot point and the point of actuation
- The sensor displacement has to be perpendicular to the line between the pivot point and the encoder position

1.3 Kinematic Structure

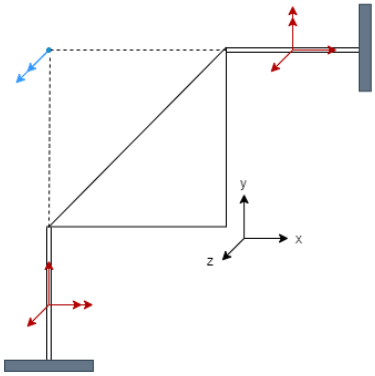

Figure 2: Kinematic Structure (Side view)

The elements used to connect the structures are two leaf springs. For each leaf spring, 3 DOFs are constrained, 2 translations and 1 rotation. In total, there are 6 constraints and 1 DOF of rotation at the point where the two leaf springs intersect. There is an over-constraint of translation in the z-direction. In Figure 2, the red arrows indicate constraints (single-head arrows for translation and double-headed arrows for rotation), while the blue double-headed arrow represents a rotational DOF about z-axis.

1.4 Dynamic Parameters

Nominal model

The Ideal Physical Model (IPM) and Free Body Diagram (FBD) of the system are seen in Figure 3 and Figure 4, where the input is generated by the VCM. The working principle of the system is a linear action of the motor which is converted into rotation.

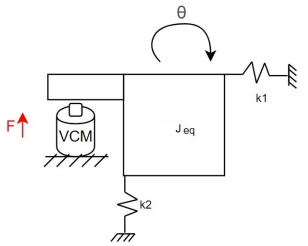

Figure 3: IPM

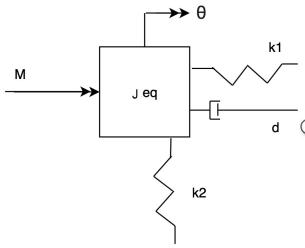

Figure 4: FBD

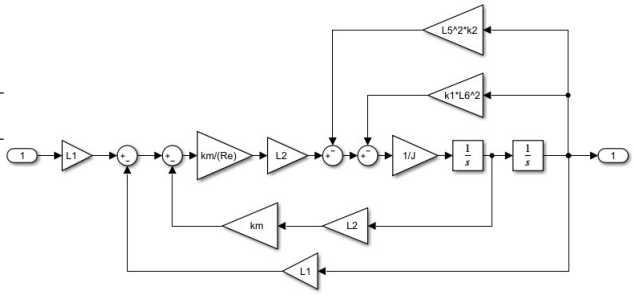

Figure 5: Nominal Block

The nominal block diagram in Figure 5 is built from the FBD. It consists of the replacement of the mechanical components into the equivalents from the Simulink library.

To find the nominal transfer function, all the stiffnesses are to be neglected, i.e, all masses and inertias are rigidly connected. Furthermore, the damping of leaf springs is not considered due to their insignificance, in comparison with damping due to back-emf. The nominal model is a basic representation of the system. The effect of inductance is not taken into consideration due to its irrelevancy in the approximation of the error in low frequency. Finally, the equation of motion is obtained from the FBD which is used to obtain the transfer function. The relations used are $F = \frac{U \cdot Km}{R}$ and $d = \frac{km^2}{R}$. The following nominal transfer Function is obtained with an input of voltage and rotation as the output. The higher damping generated is d, which is generated by the actuator due to the back-emf effect.

$$G(s) = \frac{\frac{k_m \cdot L_2}{Re \cdot J}}{s^2 + \frac{(k_m \cdot L_2)^2}{Re \cdot J} s + \frac{k_1 \cdot L_6^2 + k_2 \cdot L_5^2}{J}} \quad (1)$$

The following equation can be used to get c_1 and c_2 which are the rotational stiffness of the system. These variables have different distances L_6 and L_5 respectively, see Figure 1. Once the values of c_1 and c_2 are obtained, values of the stiffness k of the leaf springs can be calculated, for this value the radius from the centre of the body to the leaf spring's ends is used, in both cases, the radius is L_1, see Figure 1.

$$F_{max} \cdot L_k = J \cdot \ddot{\theta_r} + c_n \cdot \theta_r \qquad n = 1, 2, \qquad k = 6, 5 \quad (2)$$

$$\frac{c_n}{L_k} = \frac{F_{max}}{\theta_r} \quad (3)$$

$$k_n = \frac{c_n}{L1} \quad (4)$$

Table 1: Stiffness Values

Elements	L	c	k
Leaf spring 1	L6	7.4610	$2.1361 \cdot 10^3$
Leaf spring 2	L5	7.8390	$2.2443 \cdot 10^3$

In Table 1 can be seen the values obtained for the rotational stiffness c1 & c2 and the value of the stiffness k1 & k2.

1.5 Control Parameters

In this subsection, a suitable controller is designed for the nominal transfer function found previously. First, the reference input signal, $\theta(t)$ is analysed and used to determine the crossover frequency, ω_c that is capable of providing the maximum tracking error of 25 μrad. The tracking error is the servo error of the system. Using the ω_c found and with a few assumptions, the transfer function of the controller is determined.

Determining The Value of ω_c

Since tracking of the satellite takes place for 2 seconds, only this period of $\theta(t)$ is looked into. The graph of $\theta(t)$ is shown below in Figure 6.

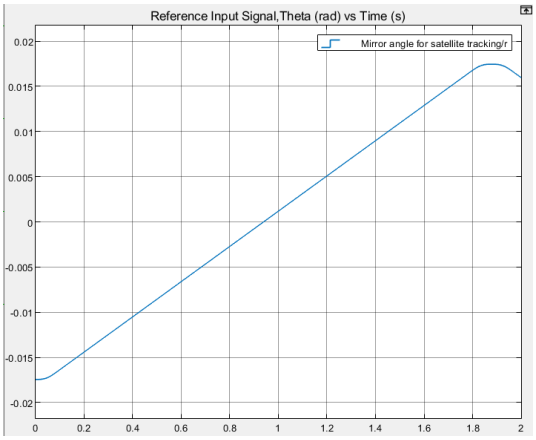

Figure 6: Reference input signal, $\theta(t)$ plotted for 2 seconds

From Figure 6, it can be seen that the constant velocity part occurs in the interval of 0.09s - 1.75s. It is within this interval that the satellite needs to be accurately tracked with the maximum servo error. Although all the maximum values of the derivatives of $\theta(t)$ do not occur at the same time, they will be taken into account for a conservative estimate. These values are extracted from the reference generator provided in Simulink and are shown below in Table 2.

For low-frequency approximations, the maximum servo error with feedforward can be predicted using the equation below. [2]

$$e_{LF,max} = k_j(1-g_1)\dddot{\theta}_{max} + k_a(1-g_2)\ddot{\theta}_{max} + k_v(1-g3)\dot{\theta}_{max} \tag{5}$$

Table 2: Maximum derivative values of $\theta(t)$ during the entire 2 seconds

$\dot{\theta}_{max}$	0.0195 rad/s
$\ddot{\theta}_{max}$	0.342 rad/s^2
$\dddot{\theta}_{max}$	12 rad/s^3

where, $k_j = \beta\frac{1}{\alpha\omega_c^3}$ $k_a = \beta\frac{\frac{d}{J}}{\alpha\omega_c^3}$ $k_v = \beta\frac{\omega_1^2}{\alpha\omega_c^3}$ $\omega_1 = \sqrt{\frac{c}{J}}$

From here, Equation 5 is rewritten to find ω_c as follows:

$$\omega_c = \sqrt[3]{\frac{\beta}{\alpha \cdot e_{LF,max}}\left((1-g_1)\dddot{\theta}_{max} + \frac{d}{J}(1-g_2)\ddot{\theta}_{max} + \omega_1^2(1-g3)\dot{\theta}_{max}\right)} \tag{6}$$

$e_{LF,max}$	25 $\times 10^{-6}$ rad
α	0.02
β	3
c	3.795e20
J	1.261 $\times 10^{17}$
d	8.389$\times 10^{17}$
g1,g2,g3	0.9

Table 3: Values for Equation 6

The value of $e_{LF,max}$ was given in the project description while the the other values in Table 4 are taken as assumptions and fined tuned to obtain favourable results for ω_c. These values are substituted into Equation 6 and the following result is obtained.

$$\omega_c = 352\,\text{rad/s} \tag{7}$$

Determining Transfer Function of Controller

Table 4: Values for Equation 8

τ_z	0.020
τ_p	4.01×10^{-4}
τ_i	0.0602
k_p	8589
m_{eq}	0.488

The next step is to determine the type of controller to be used. As an initial assumption a PID contoller is chosen. The transfer function of a PID controller is represented as follows [2]:

$$K(s) = \frac{k_p(s\tau_z + 1)}{s\tau_i(s\tau_p + 1)}(s\tau_i + 1) \tag{8}$$

where, $\tau_z = \frac{1}{\sqrt{\alpha}\omega_c}$ $\tau_p = \frac{\sqrt{\alpha}}{\omega_c}$ $\tau_i = \beta \cdot tz$ $k_p = m_{eq} \cdot \omega_c^2\sqrt{\alpha}$
$m_{eq} = \frac{J \cdot Re}{km \cdot a^2}$

The values for the variables in Equation 8 can be found in Table 4.

Stability margins

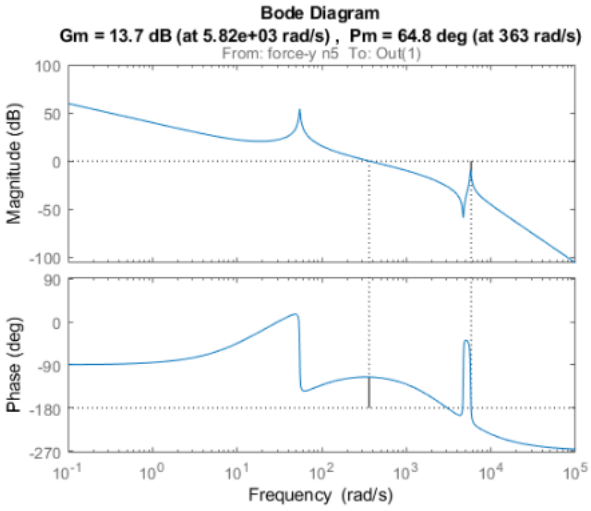

Figure 7: Open loop stability margins

The stability margins are related to the open loop system of the controller with the nominal transfer function (Equation 1). This is shown in Figure 7. Since there is no point in which the magnitude is greater than 0 db while the phase is -180 degrees, the system can be considered sable. The phase margin and gain margin are also reasonable values.

2 Design

2.1 Mechanical Design

In this subsection, the dimensions of the leaf springs are assumed, and the mechanical stresses and nominal stiffness are analysed. Stiffness, k and stresses, σ of each leaf springs are evaluated using beam theory from the course Mechanics of Materials. Leaf springs are considered as beams subjected to bending loads at the end of the beams. Using the relation between internal moment and lateral displacement of the beam, the deflection at the tip is derived as seen in Equation 9 [3]:

$$v(L) = \frac{ML^2}{2EI} + \frac{FL^2}{3EI} \tag{9}$$

- M = Moment applied at end of beam, Nm
- F = Transverse load applied at end of beam, N
- L = Length of beam, m
- E = Young's Modulus of Material 1.4310 [4], $200kN/mm^2$
- I = Area moment of inertia, m^4

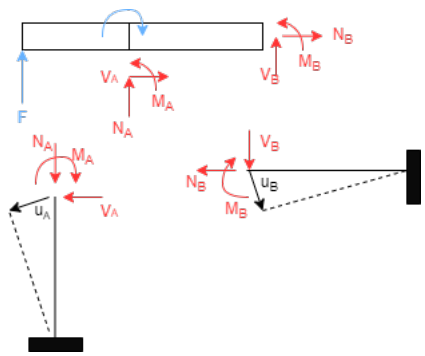

Figure 8: FBD of system

The FBD of the system is shown in Figure 8, 9 equations of equilibrium are solved to obtain the 9 unknowns V_A, V_B, M_A, M_B, N_A, N_B, u_A, u_B, and F. Given the maximum angular velocity, the maximum angle of rotation is $\theta = 39mrad$. The maximum deflections of each leaf springs are known as $u_A = u_B \approx \theta \cdot L$.

The stiffness and stresses are determined using relations in Equation 10. P is the load experienced by leaf spring, and v the deflections.

$$k = \frac{P}{v} \qquad \sigma = -\frac{M \cdot t}{I} \tag{10}$$

Table 5: Dimensions, stiffness, and stresses of leaf springs

	Length, L (m)	Width, w (m)	Thickness, t (m)	Stiffness, k (N/m)	Stress, σ (MPa)
Vertical	0.10	0.0375	0.0001	398	15.6
Horizontal	0.08	0.0375	0.0002	473	19.2

2.2 CAD Model

In this section a cad model made with the help of Solidworks 2019 are presented in Figure 9 and Figure 10.

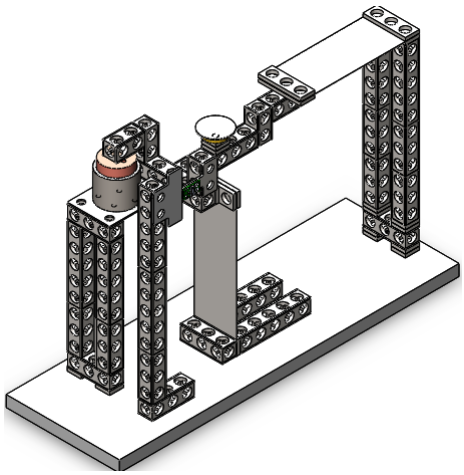

Figure 9: Isometric view

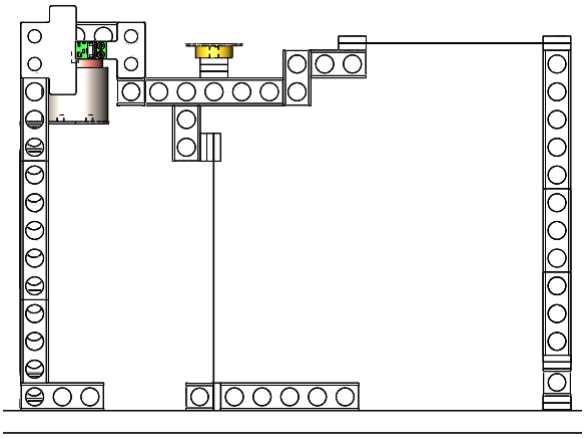

Figure 10: Side view

2.3 Frequency Response, Eigenfrequencies and Mode Shapes

In this subsection, the mechanical part as seen in the subsection above is modeled in Spacar. This is done to check the values of stiffness and stress and to accurately determine the eigenfrequencies and their relevant mode shapes.

A single node was created where the mass and inertia of all the parts supported by the leaf spring was placed (Node 1). The actuator force acts on Node 2. Node 1 is also the pivot point of the rotation. The Spacar model is shown below in Figure 11 and Figure 12.

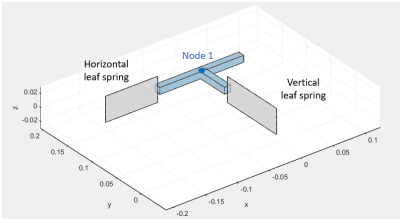

Figure 11: Spacar model

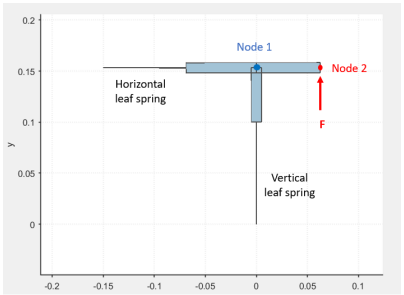

Figure 12: Side view of Spacar model

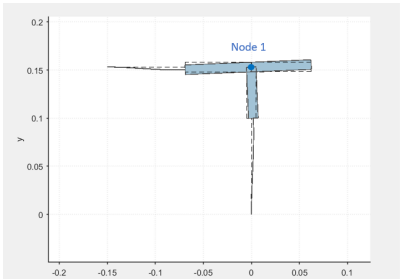

Figure 13: Spacar model showing rotation at Node 1

The rotation about Node 1 is measured and tuned to achieve the 0.039 rad required. Tuning was done by adjusting the stiffness of the 2 leaf springs by changing their dimensions. The rotation of Node 1 and bending of the leaf springs when the force, F is applied is shown below in Figure 13.

To achieve a rotation of 0.039 rad, the following values were obtained and shown below in Table 6. (Note: The subscripts "$_h$" and "$_v$" represent the horizontal and the vertical leaf springs respectively.)

Looking at the maximum stresses present it can be seen that they are well below the yield stress of the material of 400 MPa [5]. The F needed is also within limits.

A list of the eigenfrequencies of the model is shown below in Table 7. From the list it can be concluded that the crossover frequency should be between 54.97 - 990.9 rad/s. Referring to Equation 6, this condition is satisfied. All eigenfrequencies after the second eigenfreguency can be considered parasitic.

Table 6: Values used to achieve a rotation of 0.039 rad

F	0.95 N
k_h	288 N/m
k_v	457 N/m
$\sigma_{max,h}$	95.1 MPa
$\sigma_{max,v}$	30.5 MPa

Table 7: List of eigenfrequencies

	Frequency (rad/s)
1	54.97
2	990.9
3	5738
4	7360
5	9004
6	10080

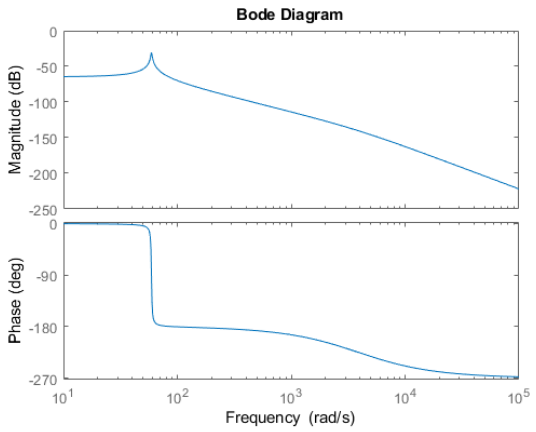

Figure 14: Frequency response of mechanical & electrical system

From Spacar, the transfer function for the mechanical plant was extracted and added to the electrical part. The transfer function was also modified to keep frequencies that were only below the nyquist frequency (using a sample time of 0.5 ms). This transfer function is shown below in Equation 11 and its frequency response is shown in Figure 14. The transfer function can be rewritten as in Equation 12 to better show the poles and zeros present. Looking at the complex pole pairs, it can be seen that the eigenfrequencies match the first three presented in Table 7.

$$G(s) = \frac{(13.66)s^4 + (1324)s^3 + (3.143e08)s^2 + (6.996e09)s + 2.954e14}{s^6 + (135.7)s^5 + (3.392e07)s^4 + (8.029e08)s^3 + (3.243e13)s^2 + (3.785e13)s + 9.767e16} \tag{11}$$

$$G(s) = \frac{11945(s^2 + 19.81s + 9.817e05)(s^2 + 77.12s + 2.203e07)}{(s + 3880)(s^2 + 5.834s + 3025)(s^2 + 19.82s + 9.818e05)(s^2 + 115.5s + 3.293e07)} \tag{12}$$

2.4 Controller Discretization

The continuous, s-domain transfer function must be converted to a z-domain in order to discretize, for it to be compatible with controllers (digital).

The transfer function of the controller,

$$K(s) = \frac{10.36s^2 + 688.4s + 8580}{2.414e - 05s^2 + 0.06018s} \tag{13}$$

For the PID-controller, discretization is performed using the Tustin method which results in the transfer function,

$$K(z) = \frac{2.687e05z^2 - 5.286e05z + 2.599e05}{z^2 - 1.104z + 0.1036} \tag{14}$$

The Bode plot is compared with that of the continuous PID-controller which is illustrated in the figure given below.

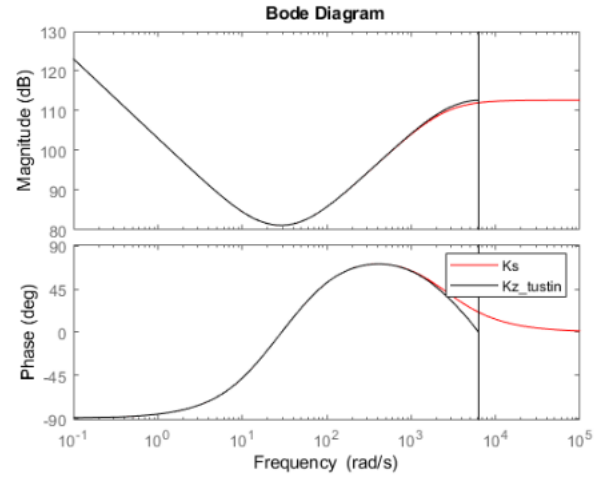

Figure 15: Bode Plot of Discretized controller TF

It is observed that increasing the sampling frequency gives a better approximation of the bode plot of the TF of the controller. For the bode plot in Figure 15, the sampling time was taken to be 27.3973 times the cross over frequency (refer Equation 7) to perfectly match it to the sampling frequency of the controller.

2.5 Effects of Parasitic Dynamics, Controller Discretization, Sampling and Delay

In this subsection an analysis of the system obtained from Spacar (Equation 11) is done. The system undergoes discretization and delay is added. The addition of these parameters to the stability margins is looked into to see if the system remains stable.

Parasitic Dynamics

The effect of the parasitic dynamics is not dangerous for the system because the ω_c of 352 rad/s is well below the first parasitic resonance frequency of 990 rad/s. This can be seen in Table 7.

Controller Discretization, Sampling and Delay

The stability margins are studied for three different cases:

Case 1: Open loop (Equation 15)

$$G_o(s) = K(s)G(s) \tag{15}$$

where K(s) is the controller (Equation 13) and G(s) (Equation 12) is the plant with the motor transfer function($\frac{1}{Ls^2+Re}$).

Case 2: Discretized open loop (Equation 16)

$$G_o(z) = K(z)G(z) \tag{16}$$

where K(z) is the discretized controller (Equation 14) and G(z) is the transfer function of the plant(Equation 12) after undergoing discretization with the method of Zero-order Hold

Case 3: Delay added to the discretized open loop (Case 2) with sampling time of 0.5 ms.

The bode plots of these three cases are plotted below in Figure 16, Figure 17 and Figure 18. The gain margin, phase margins and ω_c are shown in Table 8.

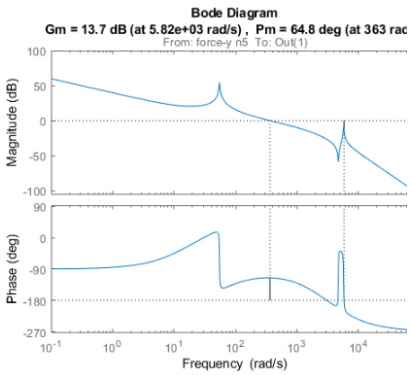

Figure 16: Case 1

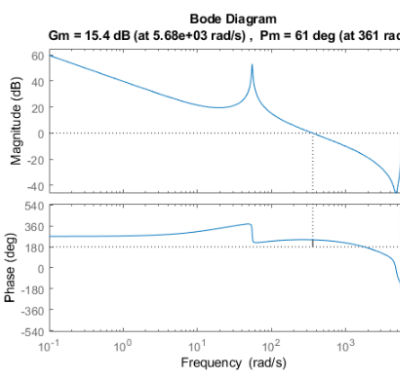

Figure 17: Case 2

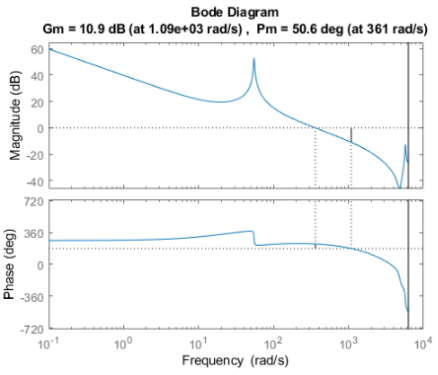

Figure 18: Case 3

Table 8

Case	Gain Margin [dB]	Phase Margin [°]	$\omega_c[rad/s]$
1. Open Loop	13	64.8	361
2. Discretized	15.4	61	363
3. Delay Added	10.9	50.6	363

From the figures and tables above it can be concluded that the system is stable, with reasonable cross over frequency and adequate stability margins. As discretization and delay is added, a decrease in the phase can be seen. Due to the use of Tustin approximation and selecting a sampling frequency which is 20 times the ω_c, this decrease is minimal at the ω_c and still provides a good value for the phase margin.

2.6 Design Limitations

The main limitations found in the mechanism would be tolerances, since leaf springs can lose their properties after continuous use. However, the controller does regulate these changes. The weight of the mechanism may be relevant in its operation, since it can misaligned the system and lose accuracy. In addition, stress applied to components can cause long-term failure. However, changing the material to obtain greater resistance may require additional use of force and we would sacrifice the efficiency of the system requiring more input.

3 Implementation

In this section, the simulink models of the controller and also the closed-loop system which are built based on the previous parts such as subsection 2.4, are illustrated and explained in detail.

3.1 Controller (Simulink)

The contoller based on the design from the previous sections is implemented in Simulink and its model can be seen in Figure 19 below. However, the discretization method used in this section is different from the previously used method (Tustin approximation). A low pass filter has been implemented that is based on Forward Euler method of approximation for discretization.
The input of the controller is the *displacement* which is obtained after a rotation-translation conversion. The input then passes through a low pass filter followed by gains - τ_i, τ_d, and τ_z. The output of the controller is a *voltage* which is capped between -24V and 24V for the electrical part, using a saturation block, after a discrete-time-integrator block.

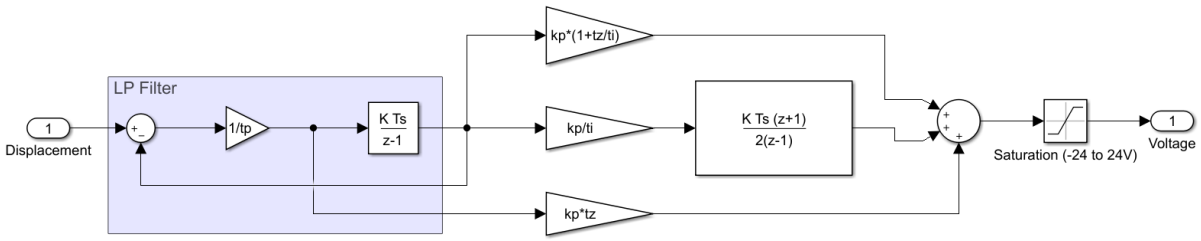

Figure 19: Controller

3.2 Simulation Model of the Closed-Loop System

The complete system, i.e, the closed-loop system can be seen as depicted in the Simulink model - Figure 20 below. The reference generator generates values for r, dr, and ddr which are then converted to displacements and are forward-fed into the controller which gives voltage as an output. This output is converted to a PWM (pulse width modulation) signal to perform ZOH discretisation and quantization of the signal. The signal is then converted back into a voltage which is sent to the electical part and followed by the plant. Displacement is fed back into the system for rectification of the error.

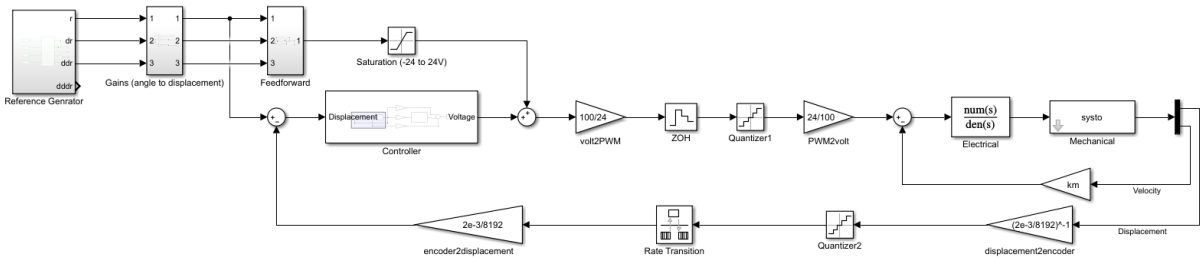

Figure 20: Simulink model of the Closed-Loop system

4 Design Verification

4.1 Static Gain and linearity

Static Gain

For this test the following settings are applied: the discrete system is used, and the output of the microcontroller is used as the input(Discrete signal). In this experiment the controller and the feedback loop is not considered, which leave the gains, quantization points and zero-order hold. Using Simulink tools the ouput data is collected,where the open loop in represented as a subsystem to get the values. The static gain is obtained by using the command dcgain(Syms), showing a dc gain of 3.6870e-5.

The Linearity of the Static Gain

Homogeneity is tested by changing the position of the amplitude, in the first test the amplitude of 0.5 is multiplied just before the system, while the second experiment has the amplitude just after the system. If the result is the same in both experiments it means that the system is linear, because it must also fulfil the second condition. The results can be seen in Homogeneity.

The second condition is additivity, where two experiments will be carried out, both will have two inputs, Step and Sinewave. In the first test, each input will go to a system and then they will be added to display the result, for the second test first the two inputs will be added (Step and Sinewave) and then they will go to a system to show the result, Figure 22 shows the results.

To comply with this condition, the results must be the same, and finally, prove that the system is linear. As a final experiment, it can be shown that the system is linear if different amplitudes are multiplied and the system shows a sequential behaviour, just like Figure 23.

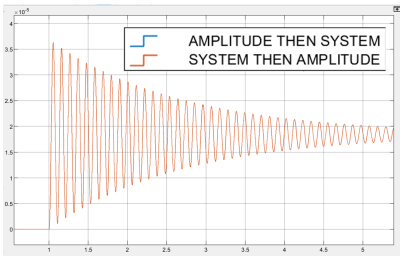

Figure 21: Homogeneity

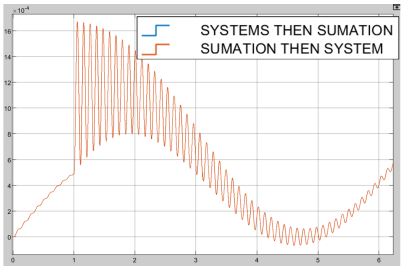

Figure 22: Additivity

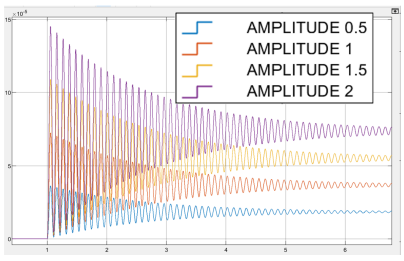

Figure 23: Different amplitudes

4.2 Frequency response

In this section the open loop system in Figure 20 is used to study frequency response.The input is a chirp input ranging form 0.01 to 50 Hz, which is applied after the controller in Figure 20. In Figure 24, the bode plot of the estimated plant is compared with the real plant. It can be seen that the low frequency gain are the same for both models. Also the phase shift is similar for both plants, but it can be noticed the effect of delay in the real plant as the frequency increases. Furthermore, the first eigen frequency of the real plant is lower than the estimated plant by around 20 rad/s, ideally the controller should be re

tuned accordingly, however the difference is considered small and the controller (eq 13) for the system will not be changed.

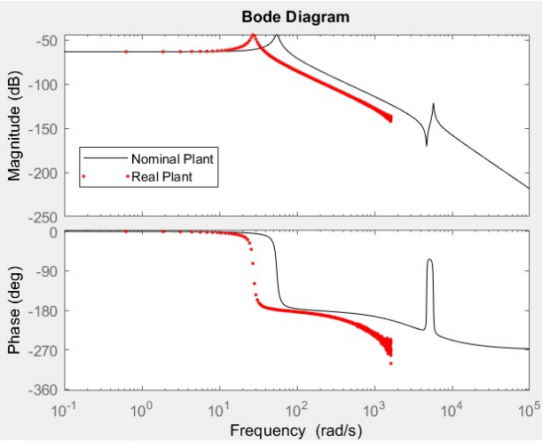

Figure 24: BODE:Real vs Nominal plants

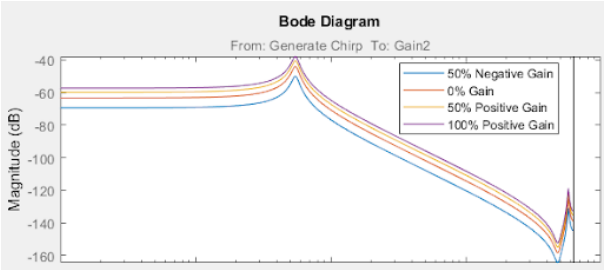

Figure 25: Affects of gain to the real plants

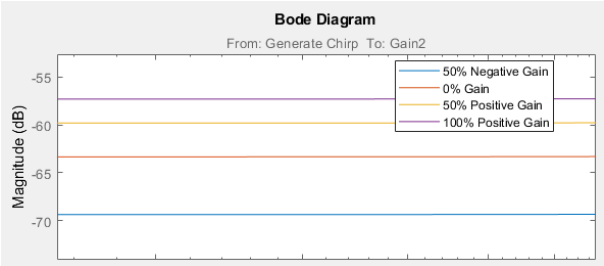

Figure 26: Close affects of gain to the real plants

In order to check the linearity of the system, Figure 25 & Figure 26 show the effect of applying a gain from less than 50% gain to 200% gain. Because the units in the gain plot are decibel and the linear behaviour is not clear at first sight. The low frequency gain is changed from decibels to linear units, this shows a difference of 0.3452e-3 between each of them, this concludes that the system is linear.

4.3 Discrete Controller

In this subsection, the frequency response with the discretized controller will be compared between the designed version and the version implemented in Simulink. Analysis will be done on the differences in gain margin, phase margin and ω_c. The frequency response of the open loop loop transfer function with all relevent parameters such as delay and quantization is shown below in Figure 27.

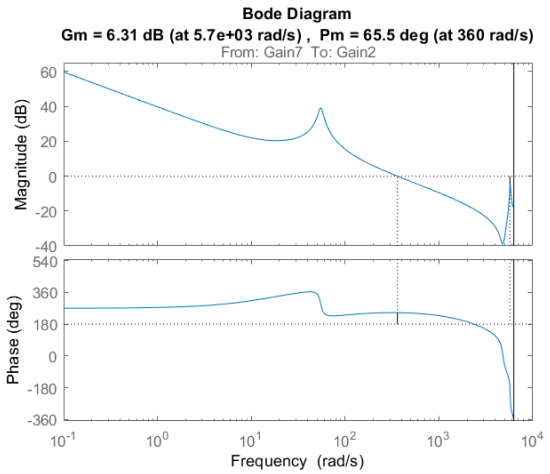

Figure 27: Frequency response of measured open loop system

Comparing to Figure 18, the gain margin and phase margin are relatively close while the ω_c is almost identical . The small differences are likely caused by the addition of non-linear blocks such as zero-order hold and quantization. Hence, the controller behaves as designed and remains stable meaning it does not require further tuning.

5 Performance Verification

5.1 Simulation results

In this section, it is verified that the designed system meets the functional requirements as stated in the first section. Simulation results are shown in figures below and tabulated in Table 9.

Table 9: System performance in relation to requirements

	Error, (rad)	Voltage, (V)	Force, (N)
Maximum value	0.0013	0.16	0.36

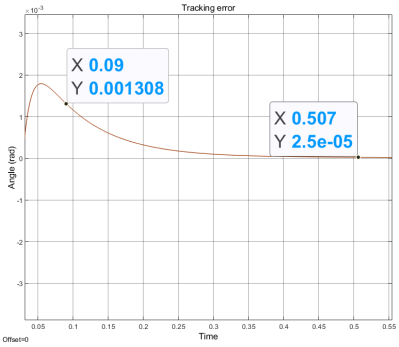

Figure 28: Tracking error

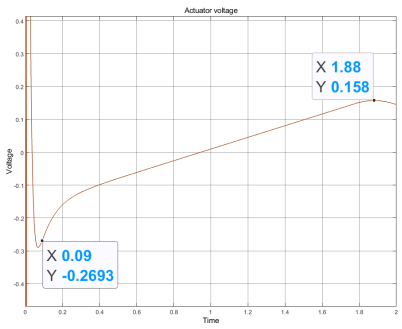

Figure 29: Voltage

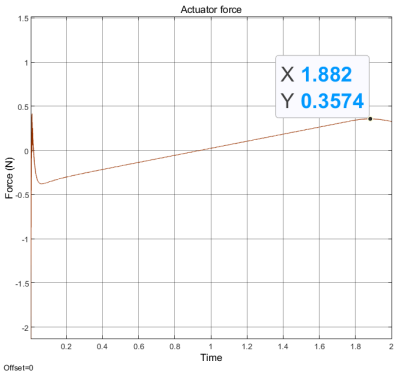

Figure 30: Actuator force

5.2 Comparison of simulation results and design analyses

In this subsection the simulations from the nominal plant and real plant is analysed focusing in the steady error , voltage and the force of each one. In this way , the results expected could be verified and the manual calculation might be checked. Moreover the effect of the inductance of the motor is considered for the real plant and feed-forward gains are added , the effect in stability and performance in the system will be visible in comparison with the nominal one. furthermore the effect of the wind up integrator might help in the limit voltage response for the real plant limiting the input for the electro-mechanical system which could be higher than 24V

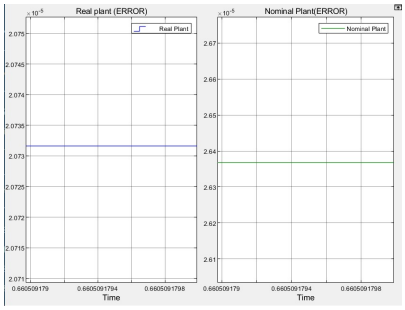

Figure 31: Force

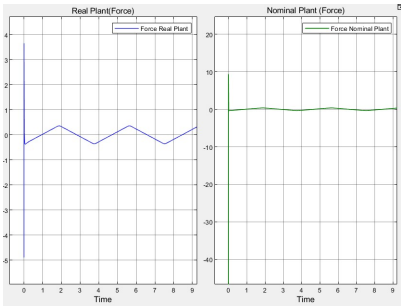

Figure 32: Force

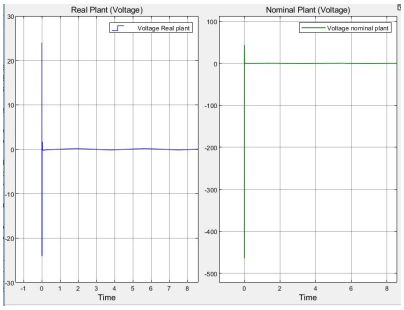

Figure 33: Voltage

5.3 Verification of system performance

The performance on functional requirements of the system is evaluated using the simulation results. As seen in Figure 28, upon entering constant velocity phase at $0.09s$, the maximum error is 1.3 $m$rad and system only achieves the required range of 25 μrad after $0.5s$. Figure 29 shows that the actuator voltage never exceeds $24V$, and in Figure 30 it can be seen that the force does not exceed limit of $4.63N$. Furthermore, robust stability is checked with equation 18.12 from the lecture notes [2], the Nyquist plot

in Figure 34 shows that the system does not go out of the unit circle, from which it can be concluded the system is robustly stable.

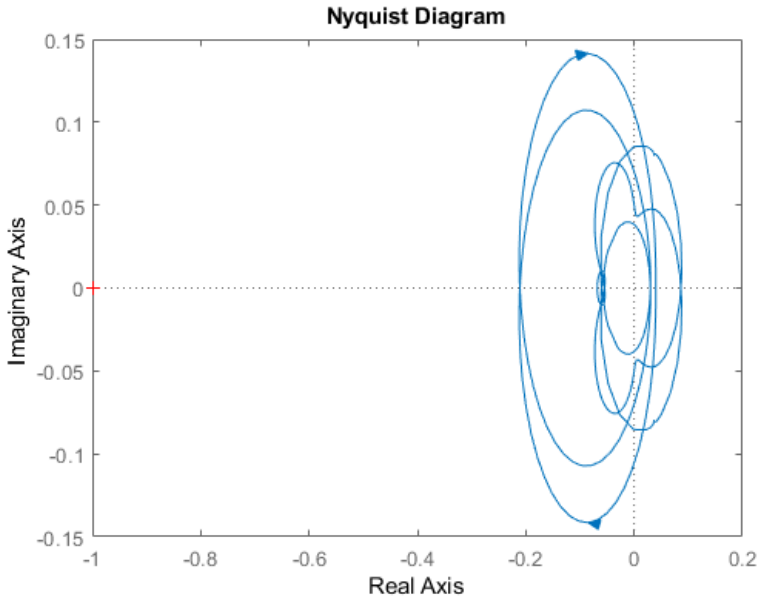

Figure 34: Nyquist plot

5.4 Evaluation & Recommendations

As observed in the previous subsections, the designed system meets most of the set requirements and gives satisfactory performance excluding settling time. A few improvements could be implemented to further optimise the system.

The designed system is stable, further steps on reducing weight and cost of the structure could be taken. However, a list of technical recommendations is as follows.

1. Two different approximation methods; Tustin and Forward-Euler were used in subsection 2.4 and subsection 3.1 respectively. The results could have been better if the same method has been used.
2. In the current simulation, anti-windup is integrated in the controller as limits. This does not pose as a significant issue for the current design as the resultant voltage is well below the limit, but for a more robust system, the anti-windup could be better integrated to the system with a feedback.
3. Equation 5 used to estimate the error of the system is a general equation derived from a simplified closed-loop model[2]. This could be revised by obtaining an equation specific to the designed system for a more accurate result.
4. The controller could be further fine-tuned to get an improved result for the settling time.

References

[1] "Free-space optical communication - Wikipedia."

[2] *Design & Control of Mechatronic Systems*, 2019.

[3] ir. Boukje de Gooijer & dr. ir. Jurnan Schilder, *Mechanics of Materials*, 2019.

[4] "Voice Coil Motor Standard Series AVM Datasheet," Tech. Rep.

[5] D. Edelstahlwerke, *1.4310 Chromium-Nickel Austenitic Stainless Steel Datasheet*, August 2007.